IEEE Access
Multidisciplinary | Rapid Review | Open Access Journal

Received June 12, 2020, accepted June 23, 2020, date of publication July 1, 2020, date of current version July 24, 2020.

Digital Object Identifier 10.1109/ACCESS.2020.3006362

Liver Cancer Detection Using Hybridized Fully Convolutional Neural Network Based on Deep Learning Framework

XIN DONG[1], YIZHAO ZHOU[1], LANTIAN WANG[1], JINGFENG PENG[2], YANBO LOU[2], AND YIQUN FAN[2]

[1]Department of Surgery, Second Affiliated Hospital, School of Medicine, Zhejiang University, Hangzhou 310009, China
[2]Department of General Surgery, Fourth Affiliated Hospital, School of Medicine, Zhejiang University, Yiwu 322000, China

Corresponding author: Xin Dong (dongxin@zju.edu.cn)

This work was supported by the Natural Science Foundation of Zhejiang Province under Grant LY17H160024.

ABSTRACT Liver cancer is one of the world's largest causes of death to humans. It is a difficult task and time consuming to identify the cancer tissue manually in the present scenario. The segmentation of liver lesions in CT images can be used to assess the tumor load, plan treatments predict, and monitor the clinical response. In this paper, the Hybridized Fully Convolutional Neural Network (HFCNN) has been proposed for liver tumor segmentation, which has been modeled mathematically to resolve the current issue of liver cancer. For semantic segmentation, HFCNN has been used as a powerful tool for liver cancer analysis. Whereas the CT-based lesion-type definition defines the diagnosis and therapeutic strategy, the distinction between cancer and non-cancer lesions is crucial. It demands highly qualified experience, expertise, and resources. However, a deep end-to-end learning approach to help discrimination in abdominal CT images of the liver between liver metastases of colorectal cancer and benign cysts has been analyzed. Our method includes the successful extraction of features from Inception combined with residual and pre-trained weights. Feature maps have been consistent with the original image voxel features, and The importance of features seemed to represent the most relevant imaging criteria for every class. This deep learning system shows the concept of illumination portions of the decision-making process of a pre-trained deep neural network, through an analysis of inner layers and the description of features that lead to predictions.

INDEX TERMS Liver cancer detection, deep learning, fully convolutional neural network.

I. INTRODUCTION

Hepatocellular carcinoma(HCC) is worldwide the other leading impact of cancer-related deaths and is the most common primary cause of hepatocellular cancer to humans [1]. Incidence rates for HCC continue to increase, unlike many other types of cancer [2]. HCC can be quickly and accurately identified and diagnosed for these patients earlier on in care with better results [3]. The need for invasive diagnostic biosophies has decreased since the quality and availability of cross-sectional imaging have enhanced and driven imaging to a more central role with a unique status, especially for primary liver tumors [4]. The liver is one of the most normal organs for CT, and metastases are a standard method for identification, diagnosis, and control of liver lesions. Liver diseases are the most common [5]. The pictures are taken before and after the injection of a competing agent with optimum lesion identification in the portal phase image [6]. Such procedures require information on lesions ' scale, shape, and accuracy [7]. Manual diagnosis and segmentation is a time-consuming process that the radiologist has to check via a 3-Dimensional Computed Tomography scan that can involve many lesions [8].

Furthermore, the scope of this challenge illustrates the need for computerized analytics to help clinicians diagnose, detect, and evaluate hepatic metastases in CT tests [9]. Due to the various contrast actions of hepatic and parenchymatic lesions, automatic identification and segmentation have been extremely challenging [10]. Besides, due to individual variances in perfusion and scan time, the image contrast between

The associate editor coordinating the review of this manuscript and approving it for publication was Wei Wei.

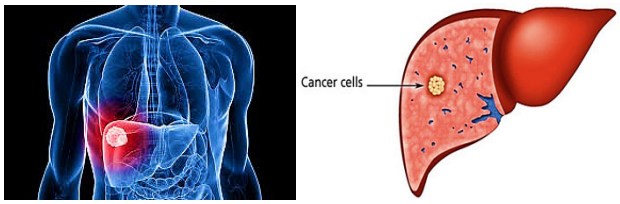

FIGURE 1. Ultrasound Image for Liver cancer cell detection [11].

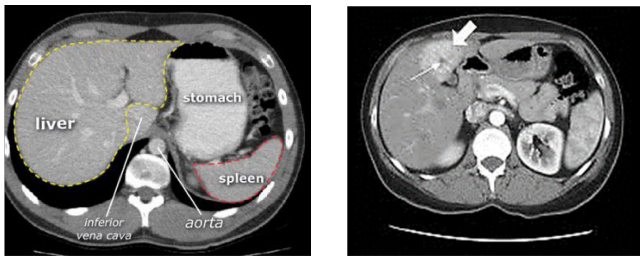

2(a) 2(b)

FIGURE 2. (a) Normal Abdominal CT scan [20] (b) Liver Lesion Image [21].

these materials can below. Figure 1 demonstrates the ultrasound imaging for liver cancer detection.

Deep learning is usually a simple way to normalize the pixels of an image to the same level. The extracted images, therefore, can reflect the features of the images themselves for pre-processed images, the nature of the extracted features dictates the exactness of the task [12] significantly. In the final step, it has concluded that the object category in the picture is the core element of deep learning, and this is the subject of most current work [13]. Machine learning algorithms have achieved better radiological efficiency and may resolve this gap in the radiological classification of different diseases [14], [15]. FCNNs (Fully Convolutional Neural Network) do not need a definition of certain radiological features to recognize images, and, unlike other machine learning approaches, they can even discover certain features that do not yet exist in current radiological practice [16]. FCNN has achieved excellent performance in various tasks, including visual recognition of the object, image classification hand-written identification of character, and more [17]. In this study, fully convolutional neural network architecture has been used to segment the liver and detect liver metastases for CT tests [18]. In the multiples sclerosis lesion segmentation, the fully convolutional architecture has recently used for medical sectors [19] (Figure 2).

Hybridized Fully convolutional networks (HFCNN) will take arbitrary inputs and generate the correct output with a corresponding efficient inference and learning. The loss function with this system is evaluated over the whole image segmentation object, as does patch-based approaches. The network handles complete images instead of patches, reducing, and need to pick reproductive patches, for avoiding redundant estimation when patches overlap, thus increasing image resolution [22]. Besides, different scales are merged by adding links that mixtures the last detection with lower layers with finer measures [23]. Such fusion can be mixed in various sizes. A lesion heat map used to diagnose is the result of this procedure [24].

The significant contribution of this paper is,

- To propose the Hybridized Fully Convolutional Neural network for liver cancer detection and segmentation.
- Designing the ensemble segmentation algorithm using a deep learning system for efficient segmentation and classification of liver tumors.
- The experimental results show that proposed HFCNN achieves high performance using the dataset from

The remainder of the paper discussed as follows: section 1 and section 2 discussed the introduction and background study of liver cancer detection. In section 3, the hybridized fully convolutional neural network has been proposed for liver cancer detection and segmentation. In section 4, the experimental results have been discussed. Finally, section 5 concludes the research study.

II. BACKGROUND SURVEY AND IMPORTANCE FEATURE OF THIS RESEARCH

Bai *et al.* [25] proposed the Multi-scale candidate generation (MCG) for the liver tumor segmentation approach on CT images. They utilized as an active contour model and 3D fractal residual network in a coarse to fine-tune the liver cancer cells. First, the liver is segmented by 3D U-Net and tumor candidates, which are identified using the MCG method. They suggest 3D FRN in respect of the candidate class. This paper proposes a variation of the superpixel segmentation approach in multiple scales and information in the neighborhood to produce candidates for segmenting the liver tumor that can require more detailed tumor data in the candidate area. It enhances the sensitivity of the network to liver tumor specifics and decreases the computational difficulty arising from redundant data. They have performed 3DIRCADb segmentation tasks, the experiment results, and comparisons with the associated research show that their advanced system can achieve a high segmentation efficiency.

Das *et al.* [26] suggested Watershed Transform and Gaussian mixture model (WT-GMM) for liver cancer recognition based on deep learning. This approach relies on the marker-controlled transformation of the watershed and the Gaussian blend model for reliable detection. The algorithm proposed is tested with clinical data from various patients in the clinical set-up in real-time. The essential advantage of this automated detection is that the deep-neural network classifier produced the best precision of 99.38 percent with negligible validation loss. The first method of application for detecting liver tumors is the use of the DNN model in the detection process. The proposed method is analyzed using an efficient way to identify the region of cancer from liver CT images that will be beneficial for the early diagnosis of symptoms in clinical and decision-making process. The estimation of the volumetric

size of the lesion is the key limit of the job, which can be constructed from various image slices in a three-dimensional mesh structure.

Ben-Cohen *et al.* [27] introduced a Fully convolutional network for liver and lesion recognition. They are investigating the FCN by way of contrast on a relatively small dataset with patch-based classification systems for CNN and sparsity. They have CT scans of 20 patients, each with a minimum of 67 lesions and 42 livers in a single slice and 22 patients with complete 3D segmentation of the liver. They have carried out 3 times cross-validation, and the results show that the FCN is superior to all other test methods. They have obtained real positive rates of 0.85 and 0.7 false-positive per case using our fully automatic algorithm that is extremely promising and clinically relevant results.

Kim and Park [28] initialized the Hybrid Feature Selection approach (HFS) based on neural network and cross-validation for liver cancer with microarray. The p-value of aptamer array response to 82 liver cancer patients and 312 healthy persons is confirmed by our system based on the artificial intelligence and 10-fold cross-validation of the neural network. Similar to the one-way ANOVA approach, the proposed method is the precision, number of features, and computation time required to identify the feature set. An increase in the number of characteristics dramatically improves diagnostic accuracy for 2 to 10 elements of both methods.

To overcome these issues, in this paper, the Hybridized Fully Convolutional Neural Network has been proposed for liver tumor detection and segmentation. Many approaches involving state-of-the-art sparse dictionary classification methods and patch-based Convolutional Neural Network have been checked. The outcomes show that the HFCNN has the best results, with data augmentation neighboring slices addition, and acceptable class weight. A small dataset and a three-fold cross-validation check have been carried out. The findings of the detection are positive.

III. HYBRIDIZED FULLY CONVOLUTIONAL NEURAL NETWORK (HFCNN)

In this paper, the Hybridized Fully Convolutional Neural Network has been proposed for liver tumor detection and segmentation. The system involves a training phase and a testing process for each neural network. The collected CT data has improved through some methods known as data augmentation during the training phase. In the neural network system, the enhanced knowledge, called input data, is then entered to obtain a qualified framework. In our feature extraction process, the testing of various layers of CNNs has tried to find a better feature extraction network. To address the limitations that are not entirely used by modern spatial 3d knowledge in the identification of neural networks. In the Proposal process for the field, the suggestions have been drawn from a pyramid structure to capture different sizes of lesions. The plan is called ROI. Whereas In this step, a texture classifier has been established to distinguish ROIs into normal and abnormal hepatic lesions. The abstract functionalities have been utilized for separating hepatocellular carcinoma (HCC), liver cysts, and hemangiomas irregular hepatic lesions at the classification detection stage. During the training phase for this project, to conducted several iterations to achieve a better model structure. In the testing stage, eventually tested the system based on the results using another batch of CT imaging. Figure 3 shows the pipeline for detecting liver lesions.

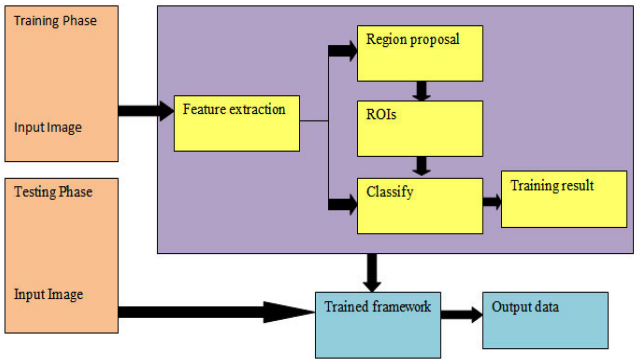

FIGURE 3. Pipeline for liver lesion detection using the proposed HFCNN.

The study used CT images of the liver over three times (enhanced, arterial, and delayed, non-contrast agent) in a clinical retrospective study. The form of the lesion cannot be determined by a mass that only occurs in a given period. Therefore, a diagnosis must be validated in comparing the difference in contrast injection between times. In the extraction process, a range of traditions has been used, well-represented in the field of computer vision extraction functions. As the number in the deep-learning network has a significant impact on final classification and recognition performance, the usual way of designing the network is as deep as possible—a false positive reduction of lung CT nodule classification CNN-based classification system. A 2D CNN-based classification system has been developed for classifying the lung nodule candidates as positive lung nodules and negative non-nodules to reduce the false positives of the initially identified lung nodule candidates. Figure 4 shows the proposed HFCNN classification system

A. MATHEMATICAL ANALYSIS USING PREPOSITION 1: AUTOENCODER MODELING

An encoder is an unsupervised feed-forward nonrecurrent neural network. Let's consider an input layer $y = (y_1, \ldots y_m)$ of dimension m, the autoencoder objective is a reconstruct y by the output y' through transforming y via successive hidden layers. Tanh is used as the activation function between the input layer y and the output layer x for given layer j. That's the following:

$$x = f_j(y) = \tanh\left(S_j y + a_j\right) \tag{1}$$

As shown in equation (1) where y and x are two vectors of size e and q correspondingly, and S_j is weight matrix of size $q \times e$, a_j an intercept vector of size q and $S_j y$ gives a vector

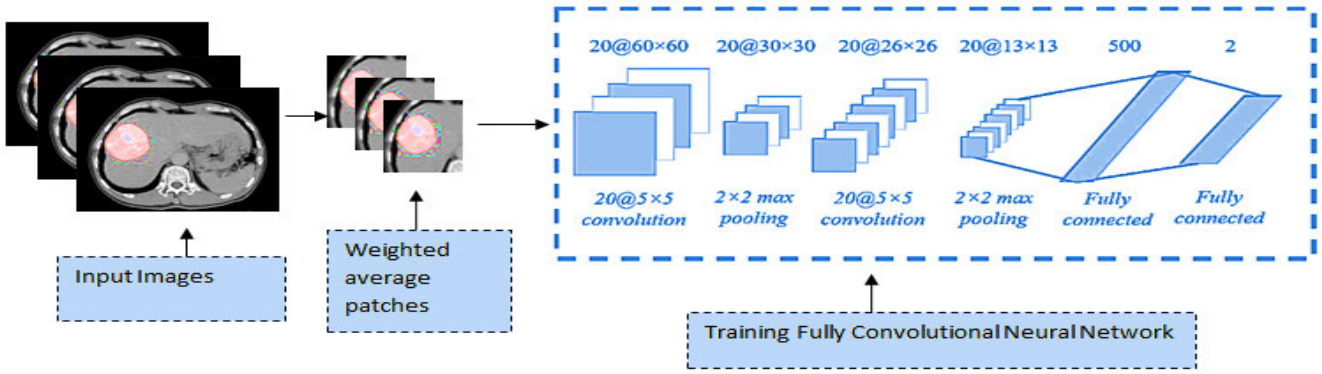

FIGURE 4. The proposed HFCNN classification system.

of size q. An autoencoder with l layers y' then expressed as,

$$y' = F_{1\to l}(y) = f_1^{\circ} \ldots f_{l-1}^{\circ} f_l(y) \tag{2}$$

As shown in equation (2) where $f_{l-1}^{\circ} f_l(y) = f_{l-1}(f_l(y))$ is the composed function of f_{l-1} with f_l. The goal is to find the different weight vectors S_j to reduce a specific objective function to train an autoencoder. As an objective function to choose log loss, which measures the error between the y input and the y' output:

$$logloss(y, y') = \sum_{l=1}^{c} \left(y_l \log\left(y_l'\right) + (1 - y_l) \log\left(1 - y_l'\right)\right) \tag{3}$$

K_1 regularization penalty has been added, β_ω on the weight vector S_j and an K_2 regularization penalty β_b on the nodes, activities to control overfitting $F_{1\to j}(y)$. Therefore, the objective function can be expressed as,

$$K(y, y') = logloss(y, y') + \sum_{j=1}^{l} \left(\beta_\omega \|S_j\|_1 + \beta_b \|F_{1\to j}(y)\|_2^2\right) \tag{4}$$

An autoencoder implemented with three hidden layers. The $\beta_\omega$and $\beta_b$values of 0.0001 and 0.001 have been set. Eventually, the gradient descent algorithm has been used to train the autoencoder at 10 epochs and 50% dropout. Epoch here is the iteration of the learning algorithm through the whole training dataset. During a cycle, each training data instance is processed once by the learning algorithm.

B. MATHEMATICAL ANALYSIS USING PREPOSITION 2: SPARSE NON-NEGATIVE MATRIX FACTORIZATION

Sparse non-negative matrix factorization (SNMF), using the sparse of every pixel in all images as a mixing degree. The sparseness function of each pixel is the norm of k_1. The goal role shall be described by:

$$\min_{D,F} \frac{1}{2} \|B - DF\|_F^2 + \beta \sum_{j=1}^{M} \|D_j\|_1^2, \quad s.t\ D, F \geq 0 \tag{5}$$

As shown in equation (5) where matrix D and matrix F are coefficients image and D_j is the row vector of D. matrix size B is $M \times N$, N is the number of dynamic images, and M is the number of pixels in the image. Frobenius norm has been used to constrain the problem in the case of the non-uniqueness of the solution in optimization. The objective role is:

$$\min_{D,F} \frac{1}{2} \|B - DF\|_F^2 + \beta \sum_{j=1}^{M} \|D_j\|_1^2 + \alpha \|F\|_1^2, \quad s.t\ D, F \geq 0 \tag{6}$$

As shown in equation (6) where $\alpha > 0$ is the attribute to suppress $\|F\|_1^2$ and $\beta > 0$ is a regularization attributes to balance the trade-off between the precision of estimation and spareness of D.

The goal function is overcome by the alternative less square (ANLS) non-negative algorithm. With the F initialization and non-negative values, the sparse NMF (SNMF) algorithm begins. The following ANLS is then iterated until convergence:

$$\min_D \left\| D\left(F\sqrt{\beta} e_{L\times 1}\right) - (B0_{L\times 1}) \right\|_F^2, \quad s.t.\ D \geq 0 \tag{7}$$

As shown in equation (7) where $e_{L\times 1} \in T^{L\times 1}$ is a column vector with all components equal, $0_{L\times 1} \in \mathbb{R}^{L\times 1}$ is a zero vector and,

$$\min_F \left\| F^R\left(D\sqrt{\alpha} J_L\right) - (B^R 0_{N\times L}) \right\|_F^2, \quad s.t.F \geq 0 \tag{8}$$

As shown in equation (8) where J_L is an identity matrix of size $L \times L$ and $0_{N\times L}$ is a zero matrix of size $N \times L$. Figure 5 shows the Sparse Non-Negative Matrix Factorization on tumor CT images.

As shown in algorithm 1 the ensemble segmentation algorithm for liver tumor detection and lesion segmentation has been analyzed. For different slices and imaging modalities, the presence of organs or structures can differ and may, therefore, require different segmentation algorithms. The proposed ensemble segmentation algorithm achieves high accuracy in detecting liver tumor detection. To classify the lesion with image features has been extracted.

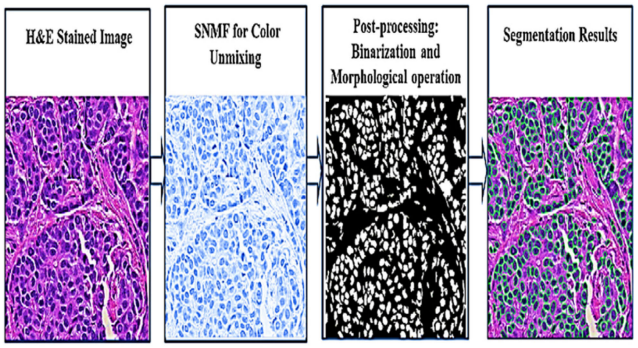

FIGURE 5. Sparse Non-Negative Matrix Factorization on tumor CT images.

Algorithm 1 Ensemble Segmentation Algorithm

Input: j,i,l,k
Output: Q, Y
For (i=0)
$x = f_j(y) = tanh(S_j y + a_j)$
For (j = 0)
$y' = F_{1\to l}(y) = f_1^{\circ} \cdots f_{l-1}^{\circ} f_l(y)$
For (l = 0)
$X = \sum_{u,g} e^{-E(u,g)}$
If (k = 0)
$q(u) = \frac{1}{X} \sum_g e^{-E(u,g)}$
Else
$q(u_j = 1 \mid g) = \rho\left(b_j + \sum_i g_i s_{ji}\right)$
(k > 1)
$Q(y, g^1, \ldots g^k) = \left(\prod_{l=1}^{k-2} Q(g^l \mid g^{l+1})\right) Q(g^{k-1}, g^k)$
End if
End for
End for
End for
End
Return

C. MATHEMATICAL ANALYSIS USING PREPOSITION 3: FULLY CONVOLUTIONAL NEURAL NETWORK

The conceptual neural network is confined to a two-layer structure in that the visible stochastic binary unit U is associated with the stochastic hidden layer unit g in which relations are formed between the levels. The hidden units are trained to identify associations of higher-order information found in a visible unit.

The visible and hidden unit joint configuration (u,g) of has energy expressed as,

$$E(u, g) = -\sum_{j \in visible} b_j u_j - \sum_{i \in hidden} a_i g_i - \sum_{j,i} u_j g_i s_{ji} \tag{9}$$

As shown in equation (9) where b_j and a_i are their biases and s_{ji} is the weight, u_i are the binary states of visible unit j and the hidden unit i. Through this energy function the network allocates a likelihood to any pair of a visible and hidden layer:

$$q(u, g) = \frac{1}{X} e^{-E(u,g)} \tag{10}$$

As shown in equation (10) where the summing over all possible pairs of hidden and visible vectors partition function X is given:

$$X = \sum_{u,g} e^{-E(u,g)} \tag{11}$$

Summing all possible hidden vectors the likelihood of the network will assign to a visible vector u is given:

$$q(u) = \frac{1}{X} \sum_g e^{-E(u,g)} \tag{12}$$

The derivative of a training vector's log-likelihood in terms of weight is expressed by:

$$\frac{\partial \log q(u)}{\partial s_{ji}} = \langle u_j g_i \rangle_{data} - \langle u_j g_i \rangle_{model} \tag{13}$$

As shown in equation (13), where Angle brackets shall be used to signify the expectations of the subscript's subsequent distribution. $\langle u_j g_i \rangle_{data}$ indicates an expectation concerning the data distribution and $\langle u_j g_i \rangle_{model}$ indicates an expectation concerning the distribution stated by the model. This entails a basic learning rule in the log-likelihood of the training data for the stochastic steepest hike:

$$\Delta s_{ji} = \epsilon \langle \langle u_j g_i \rangle_{data} - \langle u_j g_i \rangle_{model} \rangle \tag{14}$$

As shown in equation (14), where ϵ is a learning rate.

Because hidden units do not have direct connections, objective $\langle u_j g_i \rangle_{data}$ samples can easily be obtained. Given the randomly choosing trained data, u, the binary state, g_i of every hidden unit, i is set to 1 with likelihood,

$$q(g_i = 1 \mid u) = \rho\left(a_i + \sum_j u_j s_{ji}\right) \tag{15}$$

As shown in equation (15) where $\rho(y)$ is the logistic sigmoid function $\rho(y) = 1/(1 + \exp(-y))$. $u_j g_i$ is then an unbiased sample.

Since there is no direct connection between visible units, an objective study on the state of a visible unit with a hidden vector is easy to obtain:

$$q(u_j = 1 \mid g) = \rho\left(b_j + \sum_i g_i s_{ji}\right) \tag{16}$$

However, it is much more complex to get an unbiased sample of $\langle u_j g_i \rangle_{model}$. In practice learning, the gradient of a various goal function is approximated, called contrastive divergence.

This begins by putting a training vector on the states of the observable units. Then, equation (15) is used to measure all secret unit binary states in parallel. When binary states for the hidden units are chosen, a reconstruction is made by setting the u_j to 1 with equation (16). Weight change is indicated by:

$$\Delta s_{ji} = \epsilon\left(\langle u_j g_i \rangle_{data} - \langle u_j g_i \rangle_{recon}\right) \tag{17}$$

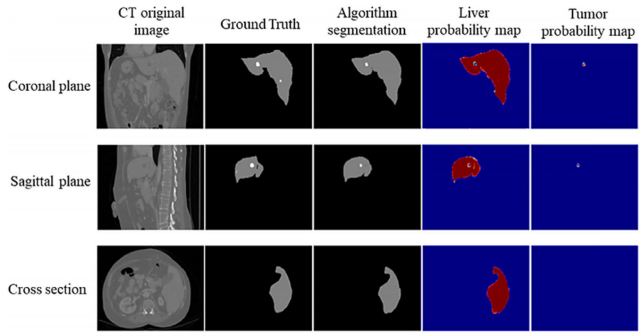

FIGURE 6. Segmentation of liver and liver tumors by three-dimensional and fully convolutional neural networks.

The fully connected convolutional neural network with k layers models the joint distribution between observed vector y and k hidden layer g^l expressed as following,

$$Q\left(y, g^1, \ldots g^k\right) = \left(\prod_{l=1}^{k-2} Q\left(g^l \left| g^{l+1}\right.\right)\right) Q\left(g^{k-1}, g^k\right) \tag{18}$$

As shown in equation (18) where $y = g^0$, $Q(g^l \left| g^{l+1}\right.)$ is a visible, hidden layer conditional distribution in a fully convolutional neural network with l level of HFCNN and $Q(g^{k-1}g^k)$ is the visible, hidden joint distribution in the FCNN.

Figure 6 shows the final segmentation of liver tumors by three-dimensional and fully convolutional neural networks. The majority of algorithms combine several techniques of segmentation and use different image indicators to boost their segmentation performance. Therefore, it may be challenging to define an algorithm. In this paper, to describe and summarize the algorithms currently available in three groups. Each category has its proper fields of operation. Researchers will combine the use of history and realistic criteria for a specific medical image segmentation task to develop appropriate algorithms. All aspects should be considered: the accuracy, complexity, effectiveness, and interactivity of the segmentation algorithm.

IV. EXPERIMENTAL RESULTS

Segmentation of liver tumor in Computed Tomography scans, involving segmentation of the liver, generation of a multi-scale candidate tumor, classification of active contour model, and tumor candidate. There have been proposals for a wide variety of machine learning approaches for segmentation liver tumors. Many CNN's have been developed in the implemented application of liver and lesion segmentation. The lesion detection data set has considerably smaller than that of the liver segmentation since, for this data set, manual segmentation masks have in 2D only. is crucial if only a few samples of training are available to train the network the necessary invariances and efficient properties. Figure 7(a) shows the test image. To produce 0.8 to 1.2 scales as the size of the lesion can be modified.

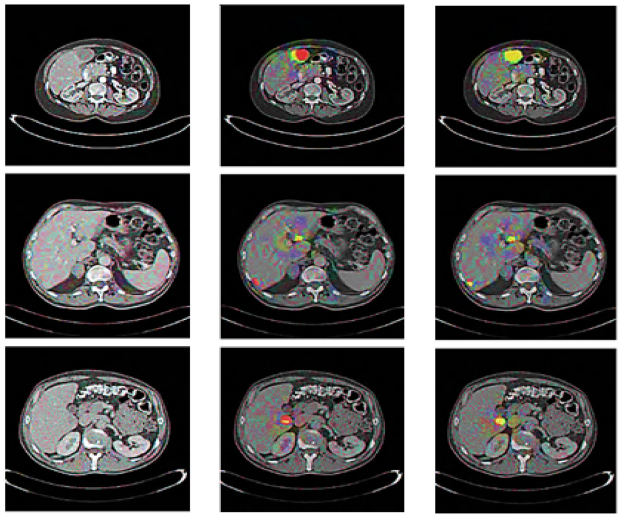

FIGURE 7. Liver tumor segmentation samples (a) test image (b) the segmentation outcome by proposed HFCNN (c) Tumor identification with lesion image.

The measurements are evenly sampled, and new photos are re-sampled using a near-neighbor method. Figure 7(b) shows the segmentation outcomes using the HFCNN method. Four measurements have been generated on a different scale for each image in our dataset. Figure 7 shows the liver tumor segmentation. Figure 7(c) shows the tumor detection with lesions.

A. TRAINING ACCURACY VS. VALIDATION ACCURACY

ROC is usually said to considerably increase the segmentation accuracy of the lesion while setting the value of the target pixels lower. The accuracy of segmentation for liver and tumor, demonstrating the efficacy of the hybrid learning process. Once the blurred limits are well segmented, large margins will boost the segmentation precision of high-time data. The hybrid property benefits segment tumors; the change is limited as small tumors are generally present in fewer slices. Figure 8 shows the training and validation exactness of the proposed HFCNN concerning the number of periods (the blue curve reveals the accuracy of training and the green curve suggests the accuracy of validation).

B. PRECISION ANALYSIS

Precision is the idea that patients are no longer treated solely by histology of the tumor, by actioning targets unique to tumor biology through a multi-omic approach. Precision medicine offers personalized attention to the machinery behind the cancer of each patient to achieve improved results for everyone. The proposed HFCNN method makes a high precision ratio when compared to other MCG, WT-GMM, FCN, HFS, and HFCNN methods. Figure 8 shows the precision ratio of the proposed HFCNN method.

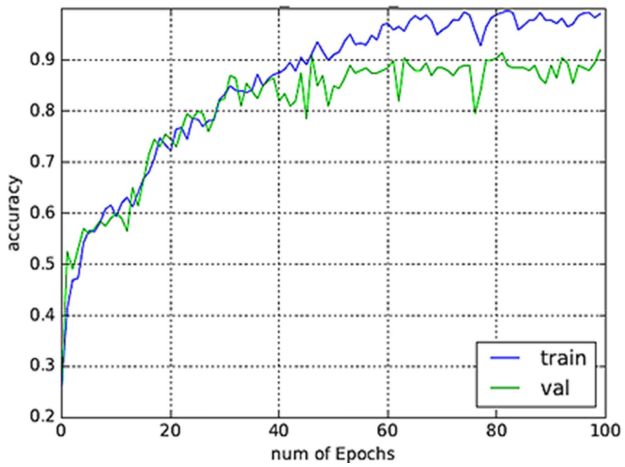

FIGURE 8. Training Accuracy vs. Validation Accuracy.

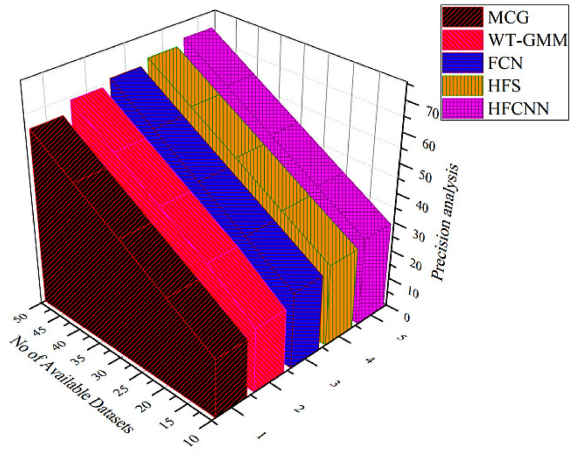

FIGURE 9. Precision Analysis Determination.

TABLE 1. Precision analysis determination.

No of Available dataset	MCG	WT-GMM	FCN	HFS	HFCNN
10	20.4	22.5	26.8	28.3	30.7
20	30.6	34.2	36.2	38.6	40.9
30	40.3	44.1	46.9	48.9	50.4
40	50.2	54.3	56.7	58.4	60.7
50	60.7	64.8	66.7	68.8	70.2

Table 1 demonstrates the precision analysis determination of the proposed HFCNN approach. Radiation therapy guidelines for liver cancer need to be met by a 3D CT scanner or tumor tracking system, strict patient accuracy, immobilization, individual image correction before radiation therapy initiation, tumor-targeting capacity, and clear dose gradients to spare tissue. The following standards need to be applied

C. DICE SIMILARITY COEFFICIENT

A common metric for assessing the precision of automated or semi-automated segmentation methods is the Dice seamlessness coefficient (DSC). The thorough validation of automated

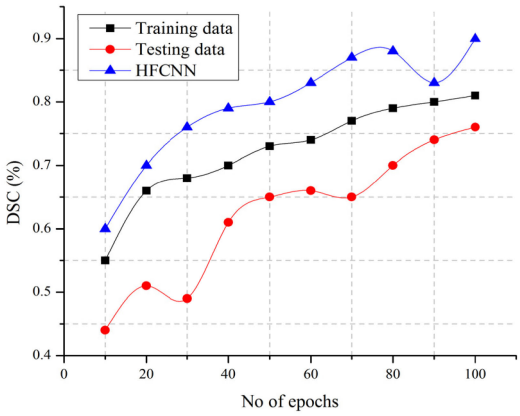

FIGURE 10. Dice Similarity Coefficient.

and semi-automated image segmentation methods is of undeniable importance, as is their outcome. Even an evaluation of image recording performance is carried out more and more by evaluating the precision of the atlas segmentation, in which the DSC is widely used.

$$C(Y, X) = \frac{2\,|Y \cap X|}{|Y| + |X|} \tag{19}$$

As shown in equation (19) where $|Y|$ indicates the cardinality of the set Y. $C\,(Y, X) \in [0, 1]$, with $C\,(Y, X) = 0$ if and only if the sets are disjoint and $C\,(Y, X) = 1$ if and only if the sets are identical.

DSC is a popular method for comparing binary segments from an image with each other. The DSC is adapted to image segmentation. Often a comparison is made with the results of automated or semi-automatic segmentation methods between the partition of the ground truth. A collection must be built for each calculating the DSC between two parts. For example, one region is identified as the foreground of each section. Figure 9 shows the dice similarity coefficient analysis.

Table 2 demonstrates the dice similarity coefficient evaluation of the proposed HFCNN method. A 3-D deep Multi-Task CNN solve has been suggested these two problems together to support hypotheses. Our dataset system has been tested and achieved an average DSC of about 91% as Segmentation Precise and an FP reduction score of almost 92%. Changes in the segments have been shown and reduction of FP over two guidelines as proof of our hypothesis.

D. RECEIVER OPERATING CHARACTERISTIC CURVE

There has two networks, one to segment the liver and the other for lesion detection. The areas around the liver, involving the various organ and tissues, has been neglected for the lesion detection training Note that a lesion-and liver-trained network has not used in our research because had two separate datasets for each mission. The pixel-wise pixel-wise feature with various weights for every class pixel has been calculated. The ROC of the proposed HFCNN has been shown in figure 10 reflects the achievement of a true positive and

TABLE 2. Dice similarity coefficient evaluation.

No of epochs	Training data	Testing data	HFCNN
10	0.55	0.44	0.6
20	0.66	0.51	0.7
30	0.68	0.49	0.76
40	0.7	0.61	0.79
50	0.73	0.65	0.8
60	0.74	0.66	0.83
70	0.77	0.65	0.87
80	0.79	0.7	0.88
90	0.8	0.74	0.83
100	0.81	0.76	0.9

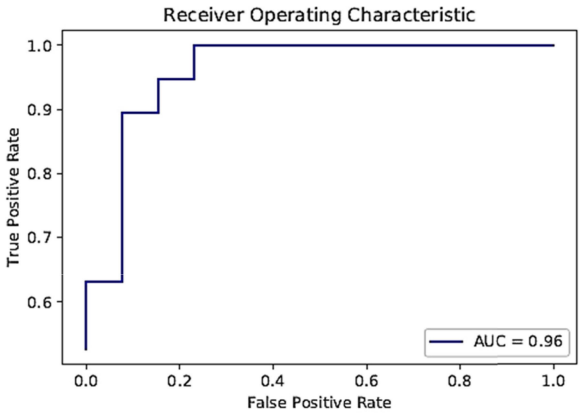

FIGURE 11. ROC curve analysis.

false positive rate algorithm, with a ROC of 0.96 given in the proposed algorithm.

E. VOLUME ERROR ANALYSIS

The volume error has been used to measure the method's sensitivity to the number of liver types. The error is stable in about 14 training forms, not at optimum value when about 23 training forms are used. The tumor burden estimate of varying image noise and patient location shows significant improvements in the precision of the segmentation of the liver even for the extreme cases of cancer. Comparative findings before and after the correction of type. Cases with extreme segmentation errors improved volume errors from 28.9% to 6.6%, whereas those with tumors improved volume error from 17.0% to 5.2%. Figure 11 shows the volume error of the proposed HFCNN method.

The network output is the likelihood of the central pixel in the input patch (target pixel). The network has two output neurons. One is the likelihood of a non-tumor (0∼1); the other is the probability of a tumor (0∼1). The output will be (0, 1 if the target pixel is tumor labeled, while the target pixel is tumor-free (1, 0) when the objective pixel is tumor-free. A cross-entropy function is used to measure the precision of the learning as a loss function. The proposed method has

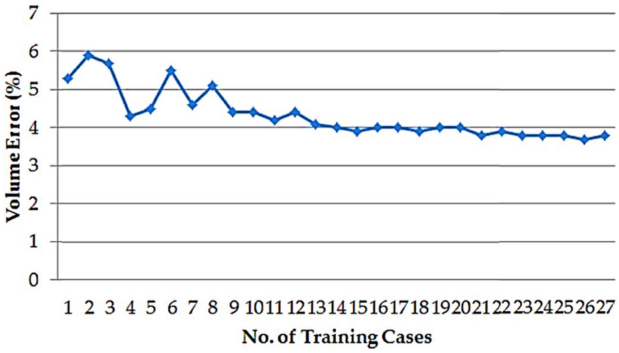

FIGURE 12. Volume error.

less complexity when compared to other existing methods. This function has been utilized to measure weight and weight loss error.

V. CONCLUSION AND ITS FUTURE OUTCOMES

This paper presents the Hybridized fully convolutional neural network (HFCNN) method for liver cancer and lesion identification and segmentation. Various layers in the neural network are utilized to extract features of medical images to improve the accuracy of the detection of medical images. 2D feature maps are combined with several slices in the feature-extraction process. The algorithm showed very accurate liver volume measurements of 97.22%. The study showed a high accuracy of the segmentation method had an average Dice coefficient of 0.92. The results show that the FCN produces the best results with data changes, adjacent slices, and appropriate class weights. Note that a limited dataset and testing have been done 3 fold cross-validation. A Convolutional Neural Network is trained to identify tumors and healthy voxels on all base-line liver maskings. CNN is used to generate the follow-up segmentation of tumors as a voxel classifier. The segmentation leaks are then eliminated in the resulting segmentation so that the final results can be obtained. The proposed HFCNN method has high accuracy in terms of identifying liver tumors.

REFERENCES

[1] L.-H. Guo, D. Wang, Y.-Y. Qian, X. Zheng, C.-K. Zhao, X.-L. Li, X.-W. Bo, W.-W. Yue, Q. Zhang, J. Shi, and H.-X. Xu, "A two-stage multi-view learning framework based computer-aided diagnosis of liver tumors with contrast enhanced ultrasound images," *Clin. Hemorheology Microcirculation*, vol. 69, no. 3, pp. 343–354, Jun. 2018.

[2] E. Vorontsov, M. Cerny, P. Régnier, L. Di Jorio, C. J. Pal, R. Lapointe, F. Vandenbroucke-Menu, S. Turcotte, S. Kadoury, and A. Tang, "Deep learning for automated segmentation of liver lesions at CT in patients with colorectal cancer liver metastases," *Radiol. Artif. Intell.*, vol. 1, no. 2, Mar. 2019, Art. no. 180014.

[3] P. Lakhani and B. Sundaram, "Deep learning at chest radiography: Automated classification of pulmonary tuberculosis by using convolutional neural networks," *Radiology*, vol. 284, no. 2, pp. 574–582, Aug. 2017.

[4] K. Yan, X. Wang, L. Lu, and R. M. Summers, "DeepLesion: Automated mining of large-scale lesion annotations and universal lesion detection with deep learning," *J. Med. Imag.*, vol. 5, no. 3, p. 036501, Jul. 2018.

[5] P. F. Christ, M. E. A. Elshaer, F. Ettlinger, S. Tatavarty, M. Bickel, P. Bilic, and W. H. Sommer, "Automatic liver and lesion segmentation in CT using cascaded fully convolutional neural networks and 3D conditional random fields," in *Proc. Int. Conf. Med. Image Comput. Comput.-Assist. Intervent.* Cham, Switzerland: Springer, Oct. 2016, pp. 415–423.

[6] P. Hu, F. Wu, J. Peng, P. Liang, and D. Kong, "Automatic 3D liver segmentation based on deep learning and globally optimized surface evolution," *Phys. Med. Biol.*, vol. 61, no. 24, pp. 8676–8698, Dec. 2016.

[7] K. Men, X. Chen, Y. Zhang, T. Zhang, J. Dai, J. Yi, and Y. Li, "Deep deconvolutional neural network for target segmentation of nasopharyngeal cancer in planning computed tomography images," *Frontiers Oncol.*, vol. 7, p. 315, Dec. 2017.

[8] K. Wu, X. Chen, and M. Ding, "Deep learning based classification of focal liver lesions with contrast-enhanced ultrasound," *Optik*, vol. 125, no. 15, pp. 4057–4063, Aug. 2014.

[9] E. Trivizakis, G. C. Manikis, K. Nikiforaki, K. Drevelegas, M. Constantinides, A. Drevelegas, and K. Marias, "Extending 2-D convolutional neural networks to 3-D for advancing deep learning cancer classification with application to MRI liver tumor differentiation," *IEEE J. Biomed. Health Informat.*, vol. 23, no. 3, pp. 923–930, May 2019.

[10] G. Chlebus, A. Schenk, J. H. Moltz, G. B. van, H. K. Hahn, and H. Meine, "Deep learning based automatic liver tumor segmentation in CT with shape-based post-processing," in *Proc. 1st Conf. Med. Imag. Deep Learn. (MIDL)*, Amsterdam, The Netherlands, 2018.

[11] *Magnetic Resonance Imaging-Visible Amonafide-Eluting Alginate Microspheres, a Novel Drug Carrier for Targeted Arterial-Infusion Chemotherapy for Liver Tumors*. Accessed: Feb. 2015. [Online]. Available: https://www.selleckchem.com/blog/Magnetic-resonance-imaging-visibleamonafide-eluting-alginate-microspheres-novel-drug-carrier-for-targetedarterial-infusion-chemotherapy-for-liver-tumors.html

[12] A. Ben-Cohen, E. Klang, A. Kerpel, E. Konen, M. M. Amitai, and H. Greenspan, "Fully convolutional network and sparsity-based dictionary learning for liver lesion detection in CT examinations," *Neurocomputing*, vol. 275, pp. 1585–1594, Jan. 2018.

[13] A. Tsuboi, S. Oka, K. Aoyama, H. Saito, T. Aoki, A. Yamada, T. Matsuda, M. Fujishiro, S. Ishihara, M. Nakahori, K. Koike, S. Tanaka, and T. Tada, "Artificial intelligence using a convolutional neural network for automatic detection of small-bowel angioectasia in capsule endoscopy images," *Digestive Endoscopy*, vol. 32, no. 3, pp. 382–390, Mar. 2020.

[14] R. Vivanti, L. Joskowicz, N. Lev-Cohain, A. Ephrat, and J. Sosna, "Patient-specific and global convolutional neural networks for robust automatic liver tumor delineation in follow-up CT studies," *Med. Biol. Eng. Comput.*, vol. 56, no. 9, pp. 1699–1713, Sep. 2018.

[15] A. Ben-Cohen, E. Klang, S. P. Raskin, M. M. Amitai, and H. Greenspan, "Virtual PET images from CT data using deep convolutional networks: initial results," in *Proc. Int. Workshop Simulation Synth. Med. Imag.* Cham, Switzerland: Springer, Sep. 2017, pp. 49–57.

[16] T. Hassanzadeh, D. Essam, and R. Sarker, "EvoU-net: An evolutionary deep fully convolutional neural network for medical image segmentation," in *Proc. 35th Annu. ACM Symp. Appl. Comput.*, Mar. 2020, pp. 181–189.

[17] M. Chung, J. Lee, M. Lee, J. Lee, and Y.-G. Shin, "Deeply self-supervised contour embedded neural network applied to liver segmentation," *Comput. Methods Programs Biomed.*, vol. 192, Aug. 2020, Art. no. 105447.

[18] X. Li, H. Chen, X. Qi, Q. Dou, C.-W. Fu, and P.-A. Heng, "H-DenseUNet: Hybrid densely connected UNet for liver and tumor segmentation from CT volumes," *IEEE Trans. Med. Imag.*, vol. 37, no. 12, pp. 2663–2674, Dec. 2018.

[19] S. Pang, A. Du, Z. Yu, and M. A. Orgun, "Correlation matters: Multi-scale fine-grained contextual information extraction for hepatic tumor segmentation," in *Proc. Pacific–Asia Conf. Knowl. Discovery Data Mining*. Cham, Switzerland: Springer, May 2020, pp. 462–474.

[20] *CT Abdomen General*. Accessed: Mar. 2017. [Online]. Available: https://www.startradiology.com/internships/general-surgery/abdomen/ct-abdomen-general/

[21] *Diagnostic Imaging Pathways—Focal Liver Lesion*. Accessed: Feb. 2016. [Online]. Available: http://www.imagingpathways.health.wa.gov.au/index.php/imaging-pathways/gastrointestinal/liver/investigation-of-a-focal-liver-nodule

[22] A. Sachse, J. U. Leike, G. L. Röling, S. E. Wagner, and W. Krause, "Preparation and evaluation of lyophilized iopromide-carrying liposomes for liver tumor detection," *Investigative Radiol.*, vol. 28, no. 9, pp. 838–844, Sep. 1993.

[23] J. S. Hong, T. Kaneko, R. Sekiguchi, K. H. Park, "Automatic liver tumor detection from CT," *IEICE Trans. Inf. Syst.*, vol. 84, no. 6, pp. 741–748, 2001.

[24] W. Huang, N. Li, Z. Lin, G.-B. Huang, W. Zong, J. Zhou, and Y. Duan, "Liver tumor detection and segmentation using kernel-based extreme learning machine," in *Proc. 35th Annu. Int. Conf. IEEE Eng. Med. Biol. Soc. (EMBC)*, Jul. 2013, pp. 3662–3665.

[25] Z. Bai, H. Jiang, S. Li, and Y.-D. Yao, "Liver tumor segmentation based on multi-scale candidate generation and fractal residual network," *IEEE Access*, vol. 7, pp. 82122–82133, 2019.

[26] A. Das, U. R. Acharya, S. S. Panda, and S. Sabut, "Deep learning based liver cancer detection using watershed transform and Gaussian mixture model techniques," *Cognit. Syst. Res.*, vol. 54, pp. 165–175, May 2019.

[27] A. Ben-Cohen, I. K. E. Diamant, M. Amitai, and H. Greenspan, "Fully convolutional network for liver segmentation and lesions detection," in *Deep Learning and Data Labeling for Medical Applications*. Cham, Switzerland: Springer, 2016, pp. 77–85.

[28] S. Kim and J. Park, "Hybrid feature selection method based on neural networks and cross-validation for liver cancer with microarray," *IEEE Access*, vol. 6, pp. 78214–78224, 2018.

XIN DONG received the M.D. and Ph.D. degrees in surgery from the School of Medicine, Zhejiang University, in June 2008. From 2015 to 2019, he has worked as the Executive Director of the Department of General Surgery, Fourth Affiliated Hospital, School of Medicine, Zhejiang University. He is currently an Attender with the Department of Surgery, Second Affiliated Hospital, School of Medicine, Zhejiang University. His current research interests include early diagnosis and comprehensive treatment for hepatobiliary pancreatic disease.

YIZHAO ZHOU is currently pursuing the Ph.D. degree in surgery with the School of Medicine, Zhejiang University. His current research interests include early diagnosis and comprehensive treatment for hepatobiliary pancreatic disease.

LANTIAN WANG received the M.D. degree in surgery from the School of Medicine, Zhejiang University, in June 2017. He is currently a Fellow with the Department of Surgery, Second Affiliated Hospital, School of Medicine, Zhejiang University. His research interests include the comprehensive treatment of hepatocellular carcinoma and the mechanism of cancer cachexia.

JINGFENG PENG received the master's degree in surgery from the School of Medicine, Zhejiang University, in June 2008. He is currently an Attender with the Department of Surgery, Fourth Affiliated Hospital, School of Medicine, Zhejiang University. His current research interest includes immunotherapy of liver cancer.

YANBO LOU received the master's degree in surgery from the West China School of Medicine, Sichuan University, in June 2010. He is currently an Attender with the Department of General Surgery, Fourth Affiliated Hospital, School of Medicine, Zhejiang University. His research interests include hepatobiliary pancreatic disease, especially focus on the early diagnosis and comprehensive treatment of pancreatic cancer.

YIQUN FAN received the master's degree in surgery from Dalian Medical University, in July 2019. He is currently a Resident with the Department of Surgery, Fourth Affiliated Hospital, School of Medicine, Zhejiang University. His current research interests include immunotherapy and comprehensive treatment for hepatobiliary pancreatic disease.